Viscoelasticity of two-layer vesicles in solution

C.-Y. David Lu[*]

Department of Chemistry and Department of Physics, Center of Theoretical Physics, National Taiwan University, Taipei 106, Taiwan

Shigeyuki Komura

Department of Chemistry, Graduate School of Science and Engineering, Tokyo Metropolitan University, Tokyo 192-0397, Japan

Kazuhiko Seki

National Institute of Advanced Industrial Science and Technology (AIST), Tsukuba 305-8565, Japan

The dynamic shape relaxation of the two-layer vesicle is calculated. In addition to the undulation relaxation where the two bilayers move in the same direction, the squeezing mode appears when the gap between the two bilayers is small. At a large gap, the inner vesicle relaxes much faster, whereas the slow mode is mainly due to the outer-layer relaxation. We have calculated the viscoelasticity of the dilute two-layer-vesicle suspension. It is found that for a small gap, the applied shear drives the undulation mode strongly while the slow squeezing mode is not much excited. In this limit, the complex viscosity is dominated by the fast-mode contribution. On the other hand, the slow mode is strongly driven by shear for a larger gap. We have determined the crossover gap, which depends on the interaction between the two bilayers. For a series of samples where the gap is changed systematically, it is possible to observe the two amplitude switchings.

PACS number(s): 82.70.Uv, 83.60.Bc, 87.16.D−, 83.80.Qr

I. INTRODUCTION

Vesicle dynamics has long been investigated both experimentally and theoretically [1–6]. The decay rate of the thermally excited shape fluctuation provides information of vesicle elasticity. The knowledge of the microscopic relaxation can also be used to predict the macroscopic rheological property of the vesicle solution [6].

The vesicles are mostly nonequilibrium system. The external perturbation, be it thermal, electrical, sonication [7,8], or flow [9,10], transforms the lamellar structure into the vesicles. In such situation, one often obtains mixture of unilamellar vesicle and multilamellar vesicles (MLV) of various sizes. However, in sharp contrast with the very detailed calculations and scattering experiments on the unilamellar vesicles, there are relatively few studies of the MLV dynamics in the literature. In this paper, we consider the two-bilayer vesicle which is the simplest MLV. We calculate the dynamic relaxation rates, as well as the rheological response of the two-layer vesicles. From the experimental point of view, it is hard to prepare vesicles with exactly two bilayers. Nonetheless, such a concrete calculation provides a clear picture of how the interaction between the two membranes affect the relaxation rates, as well as the squeezing (lubrication) flow which arises exclusively in MLV. Since our method can be extend to vesicles with more than two bilayers, a more specific calculation can be performed similarly.

The squeezing dynamics of the sandwiched solvent between the two layers has been analyzed in two related problems. This relaxation process of the flat lamellar system was calculated by Brochard and de Gennes as the "slip mode" [11] or later measured and called the "baroclinic mode" [12–14]. In the soap film system, the "squeezing mode" dispersion has been calculated and measured [15–17]. In this work, we obtain a similar relaxation, in which the solvent is squeezed between the two adjacent bilayers to relax the bilayer curvature energy and the mutual interaction energy between the two bilayers. As this mode arises only in MLV, we are interested in its dispersion relation and its coupling strength with the applied shear. Due to the strong lubrication resistance, the squeezing mode is often the slowest relaxation mode. This makes the squeezing mode an important candidate for the vesicle rheology. However, not every relaxation mode is equally excited by the applied shear. Therefore whether the shear can drive the squeezing mode with a large amplitude is an important problem to consider. In this work, we will try to build our understanding of the coupling strength through the concrete calculation.

Based on the analysis below, we find that the squeezing mode makes the dominant contribution to the complex viscosity for strongly interacting bilayers. Interestingly, when the gap between the two bilayers is smaller than a characteristic crossover gap, the fast undulation mode becomes the dominant mode for the complex viscosity. We find that the crossover gap gets very small when the bilayer interaction is strong. On the opposite limit where the bilayer has extremely weak interaction, the crossover gap becomes comparable to the inner vesicle radius.

In Sec. II, we define our model. Section III discusses the elastic force. In Sec. IV and the appendices, the flow resistance between the bilayers is solved. In Sec. V, we shall analyze the relaxation rate. In Sec. VI, we consider the viscoelasticity of the dilute vesicle suspension. Section VII includes further discussions of the results. Finally, in Sec. VIII, we provide a nontechnical summary of our results.
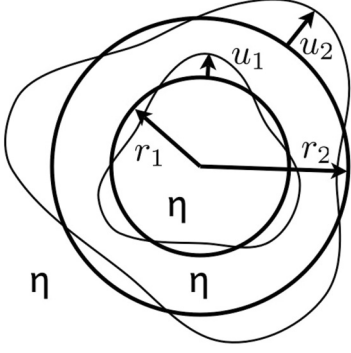
---
[*]cydlu@ntu.edu.tw

FIG. 1. The vesicle consists of two bilayers with the radius r_1 and r_2. The surrounding solvent viscosity is η everywhere.

II. THE MODEL

We consider a two-layer vesicle with two bilayers located at the spheres with mean radius r_1 and r_2 as shown in Fig. 1. The deformation of the bilayer shapes are described by the radial layer displacements u_1 and u_2 relative to the two reference spheres, respectively. Both of the bilayer membranes are surrounded by a solvent of viscosity η. Let a denote the area per molecule projected on the reference sphere and a_0 the averaged projected area per molecule. For each membrane, we define the dimensionless surface density ϕ_n ($n = 1,2$) given by the ratio a_0/a. Notice that ϕ_n becomes unity at equilibrium. In a fluctuating vesicle, ϕ_n is not uniform in general. In this work we propose the free energy of a two-layer vesicle as

$$F = \frac{(r_2^3 - r_1^3)}{3} \frac{B}{2} \int \left(\frac{u_2 - u_1}{r_2 - r_1} \right)^2 d\Omega$$
$$+ \sum_{n=1}^{2} \int \left[\gamma_n + \frac{\kappa}{2} H_n^2 + \frac{E}{2}(\phi_n - 1)^2 \right] dA_n, \quad (1)$$

where B is the layer compression modulus, γ_n the surface tension, κ the bending modulus, and E the area stretching (compression) modulus. Here both κ and E are taken to be the same for the two membranes. Moreover, $d\Omega$ is the differential solid angle, and the surface area element is approximately given by $dA_n \approx [1 + (\nabla_\perp u_n)^2/2] r_n^2 \, d\Omega$. The mean curvature H_n is given by

$$H_n \approx -\frac{2}{r_n} + \frac{2u_n}{r_n^2} + \nabla_\perp^2 u_n, \quad (2)$$

up to linear order in u_n.

Two comments should be made about the first term of Eq. (1). The compression modulus B should be a function of r_1 and r_2. In principle, a microscopic statistical model for MLV should provide the functional form. Here we focus on the layer dynamics; to build such a model is beyond the scope of this work. As a rough estimate for discussion, below in Sec. III B, we will use the B, which is calculated from the flat layers, and replace the distance d between two layers by $r_2 - r_1$. This approximation is justified for $d \ll r_2$, while it may deviate considerably when d is comparable to r_2.

The interaction term proposed here is proportional to $(u_2 - u_1)^2$, which arises naturally at small d from the square

of the strain. At large d, the curvatures and the areas for the two bilayers differ markedly. Presumably, a microscopic model may derive a more suitable weighted interaction energy, which is proportional to $[u_2 - (r_1/r_2)^\beta u_1]^2$ with a weighting exponent β. Below we present the calculation without this extra weighting factor. Nonetheless, the calculation procedure is exactly the same for the case $\beta \neq 0$.

At the dilute phase boundary of the lamellar phase, the surface tension γ_n should vanish [18]. Inside the lamellar phase, the tension depends on the applied osmotic pressure. To simplify the discussion, we shall only consider the case where the surface tension vanishes $\gamma_n = 0$. In fact, the calculation with finite surface tension can be carried out in the same way. The layer displacement u_n is related to the radial velocity v_r at $r = r_n$ by

$$\frac{\partial u_n}{\partial t} = v_r(r_n), \quad (3)$$

where we neglect the solvent permeation. The surface density obeys

$$\frac{\partial \phi_n}{\partial t} = -\frac{2v_r(r_n)}{r_n} \phi_n - \nabla_\perp \cdot [v_\perp(r_n)\phi_n], \quad (4)$$

where $\nabla_\perp$ is the two-dimensional (2D) surface derivative and $v_\perp(r_n)$ is the tangential velocity at $r = r_n$. Here we have neglected the amphiphile exchange flux between the neighboring bilayer (the amphiphile permeation).

The flow field obeys the Stokes equation, which is presented here as the form

$$\eta \nabla^2 \mathbf{v} - \nabla p = 0, \quad (5)$$

where η is the viscosity and p the pressure. Here we write down the force balance conditions that are satisfied on the two layers. The normal force balance is given by

$$-\frac{\delta F}{\delta u_n} + \sigma_{rr}(r_n^+) - \sigma_{rr}(r_n^-) = 0, \quad (6)$$

where $\sigma_{rr} = -p + 2\eta \partial_r v_r$ (r being the radial distance) and the superscripts $+$ and $-$ indicate that the stresses are evaluated at the exterior and interior of the bilayer, respectively. On the other hand, the tangential force balance is given by

$$-\frac{\delta F}{\delta \mathbf{x}_n} + \sigma_\perp(r_n^+) - \sigma_\perp(r_n^-) = 0, \quad (7)$$

where $\mathbf{x}_n$ is the 2D tangent displacement of the layers, and the 2D stress is defined as $\sigma_\perp = \hat{\theta}\sigma_{r\theta} + \hat{\varphi}\sigma_{r\varphi}$ (θ and φ being the polar and azimuthal angles, respectively).

The viscoelastic response of a dilute two-layer-vesicle suspension can be calculated by considering the stress response to an external flow at large distances from the vesicles

$$\mathbf{v}^\infty(\mathbf{r}, t) = \Gamma \nabla [r^2 Y_{20}(\theta, \varphi)] e^{i\omega t}, \quad (8)$$

where Γ is the strength of the elongational flow, $Y_{lm}(\theta, \varphi)$ are the spherical harmonics, and ω is the angular frequency. Each suspended vesicle contributes to the averaged stress. In the dilute solution, the effective complex viscosity is calculated

as [6,19]

$$\eta^* = \eta \left(1 - \frac{p_{20}^{\mathrm{II}}}{4\eta\Gamma r_2^3} \phi_v \right), \qquad (9)$$

where $\phi_v = (4\pi/3)cr_2^3$ is the volume fraction occupied by the vesicles (c is the number density of the vesicles) and p_{20}^{II} is the frequency-dependent complex coefficient of the spherical harmonic expansion of the pressure [see Eqs. (A10) and (B6) later]. The effective viscosity can also be expressed in terms of the complex modulus as $G^* = i\omega\eta^*$.

III. THE ELASTIC FORCES

A. Force expressions

The elastic forces are calculated by evaluating the derivatives $-\delta F/\delta u_n$ and $-\delta F/\delta \mathbf{x}_n$. From Eq. (4), we see that the bilayer tangential displacement and the radial displacement produce the first-order surface density perturbation as

$$\delta\phi_n = -\frac{2u_n}{r_n} - \nabla_\perp \cdot \mathbf{x}_n. \qquad (10)$$

The tangential elastic force is given by

$$-\frac{\delta F}{\delta \mathbf{x}_n} = \nabla_\perp(\delta\gamma_n), \qquad (11)$$

where the tension perturbation $\delta\gamma_n$ is induced by the surface density perturbation, i.e., $\delta\gamma_n = -E(\phi_n - 1)$. Notice that the 2D gradient has the usual component form,

$$\nabla_\perp(\delta\gamma_n) = \hat{\theta}\frac{1}{r}\frac{\partial(\delta\gamma_n)}{\partial\theta} + \hat{\varphi}\frac{1}{r\sin\theta}\frac{\partial(\delta\gamma_n)}{\partial\varphi}. \qquad (12)$$

Up to linear order in u_n and $\delta\gamma_n$, the normal force on bilayer 1 is given by

$$-\frac{\delta F}{\delta u_1} = \frac{B(r_2^3 - r_1^3)}{3(r_2 - r_1)^2}\frac{u_2 - u_1}{r_1^2} - \frac{2(\gamma_1 + \delta\gamma_1)}{r_1}$$
$$+ (\gamma_1 - \kappa\nabla_\perp^2)\left(\nabla_\perp^2 + \frac{2}{r_1^2}\right)u_1, \qquad (13)$$

whereas that for bilayer 2 is

$$-\frac{\delta F}{\delta u_2} = -\frac{B(r_2^3 - r_1^3)}{3(r_2 - r_1)^2}\frac{u_2 - u_1}{r_2^2} - \frac{2(\gamma_2 + \delta\gamma_2)}{r_2}$$
$$+ (\gamma_2 - \kappa\nabla_\perp^2)\left(\nabla_\perp^2 + \frac{2}{r_2^2}\right)u_2. \qquad (14)$$

In the large stretching modulus limit ($E \to \infty$), the tension perturbations $\delta\gamma_n$ become Lagrange multipliers, so they ensure that the right-hand side of Eq. (10) vanishes. By using Eqs. (7) and (11), the values of $\delta\gamma_n$ are determined from the viscous stress $\sigma_\perp$ (see Appendix C).

B. The bilayer interactions

There are several interactions which contribute to the layer compression modulus B. In this subsection, we indicate their physical origins and give the simplest formulae to describe them. For charged bilayers, the electrostatic interaction,

together with the counterion and coion entropy produce the free energy per area [20–22],

$$V_e = \frac{64C_s k_B T}{\kappa_D}\tanh^2\left(\frac{q\psi}{4k_B T}\right)e^{-\kappa_D d}, \qquad (15)$$

where C_s is the salt concentration, $q\psi$ the potential energy of the counterion q at the surface, κ_D the inverse of the Debye screening length, $d = r_2 - r_1$ the distance between the two surfaces, and $k_B T$ the thermal energy.

The van der Waals attraction potential per unit area can be calculated by summing the dipoles to obtain

$$V_{\mathrm{vdW}} \simeq -\frac{A}{12\pi}\left[\frac{1}{(d-\delta)^2} + \frac{1}{(d+\delta)^2} - \frac{2}{d^2}\right], \qquad (16)$$

where A is the Hamaker constant and δ is the membrane thickness. A more complicated Lifschitz theory calculation can provide a more accurate description [20–23]. The sum of these two interactions consists the standard DLVO theory. When the electrostatic repulsion and van der Waals attraction stabilize MLV, B can be evaluated from

$$B = d\frac{\partial^2(V_e + V_{\mathrm{vdW}})}{\partial d^2}. \qquad (17)$$

For a flexible bilayer where the undulation entropy depends strongly on the membrane separation d, Helfrich estimated the free energy per area and B by a self-consistent argument to obtain [21,24]

$$B = c_0\frac{(k_B T)^2}{\kappa d^3}, \qquad (18)$$

where c_0 is an order unity numerical constant. In the following examples below, we use $c_0 = 36/\pi^2$. When the van der Waals interaction becomes important, a more elaborate calculation is required to combine the undulation entropy and the van der Waals attraction [25].

IV. THE NORMAL FORCE BALANCE

Using the spherical harmonic expansion, the Stokes equation can be solved in terms of the radial functions, which are simple polynomial of the radius. The detailed calculation is presented in Appendix A. In general, the solution depends on the boundary velocities, which are the velocities of the membranes and the applied external shear. In the usual case where the bilayers have a large stretching modulus E, we can simplify the discussion by considering the large stretching modulus limit $E \to \infty$. In this limit, the surface density approaches unity, and the combinations $E(\phi_n - 1)$ become the Lagrange multipliers to ensure that surface densities are constant. Hence, the constant E can be eliminated. The detailed calculation is presented in Appendix B. At the boundaries, this limit also turns the tangential velocity into the function of the normal velocity. This means that the normal stresses $\sigma_{rr}(r_n^+)$ and $\sigma_{rr}(r_n^-)$, as well as the tension perturbation $\delta\gamma_n$, are all proportional to the bilayer normal velocities and the external shear. The detailed calculation is presented in Appendix C.

The bilayer displacements and velocities are expanded as the sum of the spherical harmonics $Y_{lm}(\theta,\varphi)$ times the time-varying amplitudes, i.e., $u_n(\theta,\varphi) = u_n Y_{lm}(\theta,\varphi)$ and

$v_r(r_n,\theta,\varphi) = v_n Y_{lm}(\theta,\varphi)$. Without cluttering the notation with the angular quantum numbers l and m, hereafter we use u_n and v_n to express the time-varying amplitudes for an arbitrary set of (l,m). After performing some calculations to express σ_{rr} and $\delta\gamma_n$ by v_n [see Eqs. (C1), (C5), (B4), (B6), and (B9)], we find that the normal force balance Eq. (6) at r_1 and r_2 can be written as

$$\mathbf{E} \cdot \begin{pmatrix} r_1^2 u_1 \\ r_2^2 u_2 \end{pmatrix} + \mathbf{D} \cdot \begin{pmatrix} r_1^2 v_1 \\ r_2^2 v_2 \end{pmatrix} = 20\eta\Gamma e^{i\omega t}\delta_{l2}\delta_{m0}\hat{\mathbf{e}}_2, \quad (19)$$

where $\hat{\mathbf{e}}_2 = (0,1)$. Here we prefer to use the variables $r_1^2 u_1$ and $r_2^2 u_2$ which make the matrices $\mathbf{E}$ and $\mathbf{D}$ symmetric. With this variable choice, the free energy per solid angle is then the quadratic form of $\mathbf{E}$. The components of the matrix $\mathbf{E}$ are given by

$$E_{11} = \frac{B(1-\rho^3)}{3r_2^3(1-\rho)^2\rho^4} + \frac{(\gamma_1 r_2^2\rho^2 + \kappa\hat{L}^2)(\hat{L}^2 - 2)}{r_2^6\rho^6},$$

$$E_{12} = -\frac{B(1-\rho^3)}{3r_2^3(1-\rho)^2\rho^2}, \quad E_{21} = E_{12}, \quad (20)$$

$$E_{22} = \frac{B(1-\rho^3)}{3r_2^3(1-\rho)^2} + \frac{(\gamma_2 r_2^2 + \kappa\hat{L}^2)(\hat{L}^2 - 2)}{r_2^6},$$

where have defined $\rho = r_1/r_2 \ (\leqslant 1)$ and

$$\hat{L}^2 = -\frac{1}{\sin\theta}\frac{\partial}{\partial\theta}\left(\sin\theta\frac{\partial}{\partial\theta}\right) - \frac{1}{\sin^2\theta}\frac{\partial^2}{\partial\varphi^2}, \quad (21)$$

whereas the components of the matrix $\mathbf{D}$ are

$$D_{11} = \frac{\eta r_2^{4l+1}(2l+1)}{G_0(l^2+l)}[-(l+1)^2(4l^2-1)\rho^{2l+1}$$
$$+ (l^2-1)(2l-1)(2l+3)\rho^{2l-1}$$
$$+ (l-1)^2(4l^2+8l+3)\rho^{2l-3} + (8l^2+8l-4)\rho^{-2}],$$

$$D_{12} = \frac{\eta r_2^{4l+1}(4l+2)}{G_0(l^2+l)}[(2l^3+5l^2+l-2)(\rho^{3l+2}-\rho^{l-1})$$
$$+ (2l^3+l^2-3l)(\rho^{l+1}-\rho^{3l})],$$

$$D_{21} = D_{12},$$

$$D_{22} = \frac{\eta r_2^{4l+1}(2l+1)}{G_0(l^2+l)}[-(l+2)^2(4l^2-1)\rho^{2l+4}$$
$$+ 2l(l+2)(2l-1)(2l+3)\rho^{2l+2}$$
$$+ l^2(4l^2+8l+3)\rho^{2l} + (8l^2+8l-4)\rho], \quad (22)$$

where

$$G_0 = r_2^{4l+4}[4\rho + 4\rho^{4l+3} - (2l+1)^2\rho^{2l+4}$$
$$- (6 - 8l - 8l^2)\rho^{2l+2} - (2l+1)^2\rho^{2l}]. \quad (23)$$

Notice that the components of $\mathbf{D}$ are the product of η/r_2^3 and the functions of ρ and l.

When the two bilayers are well separated, i.e., $r_1 \ll r_2$, they are not hydrodynamically coupled. In this limit, D_{12} and D_{21} become small, and we recover the isolated vesicle damping given by [4–6]

$$D_{nn} = \frac{\eta(2l+1)(2l^2+2l-1)}{r_n^3 l(l+1)}. \quad (24)$$

For the more general bilayer interaction which is proportional to $B[u_2 - (r_1/r_2)^\beta u_1]^2$, the similar calculation will give rise to an extra factor $\rho^{2\beta}$ for the B term in E_{11}, and an extra factor ρ^β for the B terms in E_{12} and E_{21}. The form of E_{22} is not affected.

V. RELAXATION SPECTRUM

The relaxation rates, denoted as $\Omega_j \ (j = 1,2)$, are the eigenvalues of the matrix $\mathbf{D}^{-1} \cdot \mathbf{E}$. The normal force balance condition Eq. (6) on the two bilayers gives the eigenvector equation

$$\mathbf{D}^{-1} \cdot \mathbf{E} \cdot \mathbf{d}_j^R = \Omega_j \mathbf{d}_j^R, \quad (25)$$

where $\mathbf{d}_j^R$ are the (nonorthogonal) right eigenvectors. To work with the orthogonal eigenvectors, here we define the symmetric decay rate matrix,

$$\mathbf{M} = \mathbf{D}^{-1/2} \cdot \mathbf{E} \cdot \mathbf{D}^{-1/2}, \quad (26)$$

which has the (normalized) eigenvectors $\mathbf{d}_j$,

$$\mathbf{M} \cdot \mathbf{d}_j = \Omega_j \mathbf{d}_j. \quad (27)$$

Here the eigenvalues are the same as in Eq. (25), and $\mathbf{d}_j$ is proportional to $\mathbf{D}^{1/2}\mathbf{d}_j^R$. We can decompose the decay rate matrix as

$$\mathbf{M} = \Omega_1\mathbf{d}_1\mathbf{d}_1 + \Omega_2\mathbf{d}_2\mathbf{d}_2, \quad (28)$$

which will be used in the later discussion. Hereafter, the faster and the slower rates are denoted by Ω_1 and Ω_2, respectively.

The full expression of the decay rates are straightforward but complicated. Hence, we shall obtain some simplified expressions to gain some understanding on the nature of the relaxation. We, first, discuss the fast mode Ω_1. When $\rho = 1$, the fast undulation mode has a well-known dispersion relation [3,4,6],

$$\Omega_0 = \frac{2\kappa(l-1)l^2(l+1)^2(l+2)}{\eta r_2^3(2l+1)(2l^2+2l-1)}, \quad (29)$$

where the bending modulus is doubled as there are two bilayers. For ρ slightly less than unity, a series expansion can be made if desired. For $\rho \ll 1$, the decay rate can be approximated by

$$\Omega_1 \approx \frac{E_{11}}{D_{11}}. \quad (30)$$

This corresponds to a simple picture that the fast mode consists mainly the inner bilayer relaxation, whereas the outer bilayer does not move much.

Next we consider the slow mode Ω_2. When $\rho \approx 1$, the slow mode can be approximately obtained by the series expansion of $1 - \rho$. Based on the relation $\Omega_1 + \Omega_2 = \text{tr}(\mathbf{D}^{-1} \cdot \mathbf{E})$, in which Ω_2 only starts from the second-order term, we get $\Omega_1 \simeq \text{tr}(\mathbf{D}^{-1} \cdot \mathbf{E})$ for the zeroth and the first-order terms. Because the product $\Omega_1\Omega_2$ is given by $\det(\mathbf{D}^{-1} \cdot \mathbf{E})$, we use the leading two terms of $\det(\mathbf{D}^{-1} \cdot \mathbf{E})/\Omega_1$ to obtain

$$\Omega_2 \approx \frac{Bl(l+1)}{12\eta}(1-\rho)^2(2-\rho)$$
$$+ \frac{\kappa(l-1)l^2(l+1)^2(l+2)}{24\eta r_2^3}(1-\rho)^3. \quad (31)$$

The leading term $(B/12\eta)(1-\rho)^2 l(l+1)$ is similar to the slip mode of the planar smectic, which has the decay rate $(B/12\eta)d^2 q_\perp^2$, where $q_\perp$ is the wave vector projected onto the bilayer plane [11]. This expression is also analogous to the squeezing-mode dispersion obtained for soap film [15,16]. In the other extreme of $\rho = 0$, the slow mode has the dispersion such that

$$\Omega_2 \approx \frac{\left[B + 3(l-1)l(l+1)(l+2))\kappa/r_2^3\right]l(l+1)}{3\eta(2l+1)(2l^2+2l-1)}. \quad (32)$$

If we set the shear perturbation as $l = 2$, the numerator contains a factor $B + 72\kappa/r_2^3$. Hence, the dimensionless parameter Br_2^3/κ becomes important when its value is much larger than 72.

We now discuss another approximate expression for the slow mode valid for the whole range of ρ. Since the sum of the two decay rates $\Omega_1 + \Omega_2 = \mathrm{tr}(\mathbf{D}^{-1} \cdot \mathbf{E})$ is dominated by the fast mode for any ρ, the slow mode can be approximated by the ratio

$$\Omega_2 \approx \frac{\det(\mathbf{D}^{-1} \cdot \mathbf{E})}{\mathrm{tr}(\mathbf{D}^{-1} \cdot \mathbf{E})}$$
$$= \frac{E_{11}E_{22} - E_{12}E_{21}}{E_{11}D_{22} - E_{12}D_{21} + E_{22}D_{11} - E_{21}D_{12}}. \quad (33)$$

When the inner bilayer 1 relaxes fast, one can apply the adiabatic approximation to the fast relaxing inner membrane. The approximated expression has even a simpler denominator given by

$$\Omega_2 \approx \frac{E_{22} - E_{21}(E_{12}/E_{11})}{D_{22} - D_{21}(E_{12}/E_{11})}. \quad (34)$$

In Fig. 2, we plot the decay rates as a function of $\rho = r_1/r_2$ for $l = 2$, keeping a constant B. The two solid lines represent
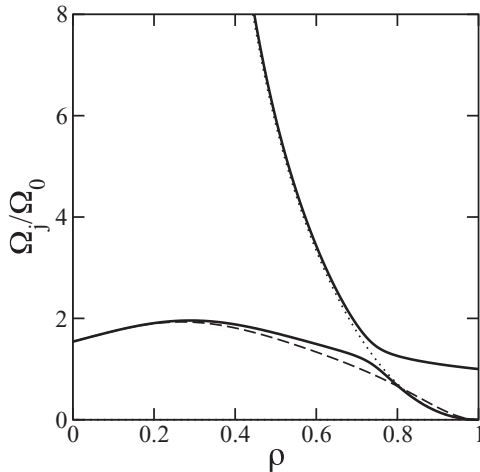

FIG. 2. The scaled relaxation rate Ω_j/Ω_0 as a function of the dimensionless size ratio $\rho = r_1/r_2$ between the two layers. Here Ω_0 is the vesicle relaxation rate with the rigidity 2κ given by Eq. (29). The two solid lines represent the two vesicle relaxation rates Ω_1 and Ω_2 obtained numerically. The dotted line is an approximation for the fast mode given by Eq. (30). The dashed line represents the approximate slow relaxation rate Ω_2 given by Eq. (34). In this plot, we set $B = 600\,\mathrm{J/m^3}$, $\kappa = k_\mathrm{B}T = 4 \times 10^{-21}\,\mathrm{J}$, $\eta = 10^{-3}\,\mathrm{Pa\,s}$, $r_2 = 10^{-7}\,\mathrm{m}$, $l = 2$, so $Br_2^3/\kappa = 150$.

the numerical calculated decay rates. The upper one is the fast mode Ω_1, which has the limit Ω_0 at $\rho = 1$. It coincides with the approximation Eq. (30) (dotted line) for $\rho < 0.6$. The lower solid line represents the slow mode Ω_2. The approximate slow rate Eq. (34) follows qualitatively the exact value of Ω_2 for the full range of ρ. It also coincides with Eq. (32) in the limit of $\rho = 0$. Incidentally, the inner layer relaxation Eq. (30) also fits the slow mode Ω_2 at $\rho \approx 1$.

Figure 2 is useful to illustrate the nature of the relaxation for the fast and slow modes. In a real system, B is a function of r_1 and r_2 (or ρ and r_2), which is difficult to keep as a constant. One will make a plot with a function for B which is suitable for the specific MLV system. If one uses the flat layer formulas described in Sec. III B as approximations, caution should be kept for the accuracy at small ρ. Given an accurate function for B, together with the proper weighting factor (to combine $\rho^{2\beta}$ and ρ^β factors in $\mathbf{E}$), the above decay rate approximations should work better.

VI. VISCOELASTICITY

We now consider two-layer vesicles under the external oscillatory shear flow. Rearranging Eq. (9) together with Eq. (B6), we obtain

$$\frac{\eta^*/\eta - 1}{\phi_\mathrm{v}} = \frac{5}{2} - \frac{v_2}{r_2\Gamma e^{i\omega t}}. \quad (35)$$

It is apparent that the dilute hard-sphere limit is recovered when $v_2 = 0$. By putting $u_n = v_n/i\omega$ and solving Eq. (19) for v_2, we obtain

$$\frac{\eta^*/\eta - 1}{\phi_\mathrm{v}} = \frac{5}{2} - i\omega\frac{20\eta}{r_2^3}\hat{\mathbf{e}}_2 \cdot (\mathbf{E} + i\omega\mathbf{D})^{-1} \cdot \hat{\mathbf{e}}_2, \quad (36)$$

where one should set $l = 2$ for the matrices $\mathbf{E}$ and $\mathbf{D}$. Here $\hat{\mathbf{e}}_2$ appears twice, because the shear directly affects the bilayer 2 through Eq. (19), and the velocity of the bilayer 2 carries the stress contribution of the vesicle according to Eqs. (9) and (B6).

Considering the high-frequency limit, we now define the dimensionless shear coupling strength S and the shear deformation unit vector $\hat{\mathbf{s}}$ by

$$S^{1/2}\hat{\mathbf{s}} = \left(\frac{20\eta}{r_2^3}\right)^{1/2}\mathbf{D}^{-1/2} \cdot \hat{\mathbf{e}}_2. \quad (37)$$

Notice that S and $\hat{\mathbf{s}}$ depend only on the ratio ρ as long as we fix to $l = 2$. As shown in Fig. 3, S is weakly dependent on ρ because its value varies only between 2.1 and 2.19. Hence the right-hand side of Eq. (36) varies between 0.31 and 0.4, whereas the hard-sphere case gives 2.5. This means that, at high frequencies, the coupling of a vesicle to the flow is weaker compared to that of a hard sphere.

The high-frequency viscosity asymptotically approaches

$$\eta^\infty = \eta\left[1 + \left(\tfrac{5}{2} - S\right)\phi_\mathrm{v}\right] = \eta^0 - \eta S\phi_\mathrm{v}, \quad (38)$$

where $\eta^0 = \eta[1 + (5/2)\phi_\mathrm{v}]$. Using the eigenmode decomposition $\mathbf{I} = \mathbf{d}_1\mathbf{d}_1 + \mathbf{d}_2\mathbf{d}_2$, we can separate the viscosity contributions from each mode as

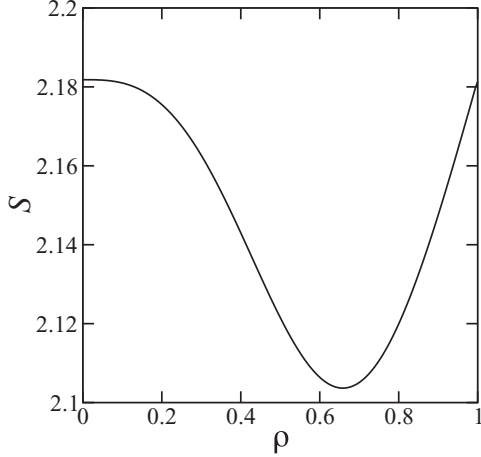$$\eta_j = S\eta(\hat{\mathbf{s}} \cdot \mathbf{d}_j)^2, \quad (39)$$

FIG. 3. The shear coupling strength S defined by Eq. (37) as a function of the dimensionless size ratio ρ between the two layers.

so we have

$$\eta S = \eta_1 + \eta_2. \tag{40}$$

The full expression for the complex viscosity then is given by

$$\eta^*(\omega) = \eta^0 - \phi_v \sum_{j=1}^{2} \eta_j \frac{i\omega}{i\omega + \Omega_j}. \tag{41}$$

The relative strength of the two modes are shown in Fig. 4. Alternatively (but equivalently), the complex modulus can be expressed as

$$G^*(\omega) = i\omega\eta^\infty + \phi_v \sum_{j=1}^{2} G_j \frac{\omega^2 + i\omega\Omega_j}{\omega^2 + \Omega_j^2}, \tag{42}$$

where the two modes have the positive amplitudes $G_j = \Omega_j \eta_j$.

Even for different bilayer interaction strength B, we always find that the slow mode has the larger viscosity amplitude at $\rho \approx 0$, and smaller one at $\rho \approx 1$. The latter is reasonable because the shear perturb the two bilayers similarly for $\rho \approx 1$,
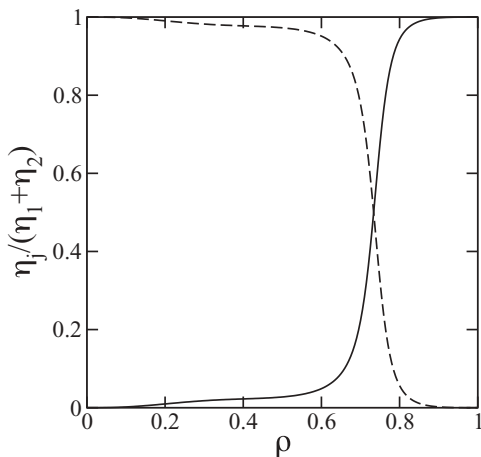

FIG. 4. The relative viscosity strengths defined by Eq. (39) as a function of the dimensionless size ratio ρ between the two layers. The solid and the dashed lines corresponds to η_1 and η_2, respectively. We chose the value $Br_2^3/\kappa = 150$. The crossing of the two modes occurs at $\rho^* \approx 0.733$.
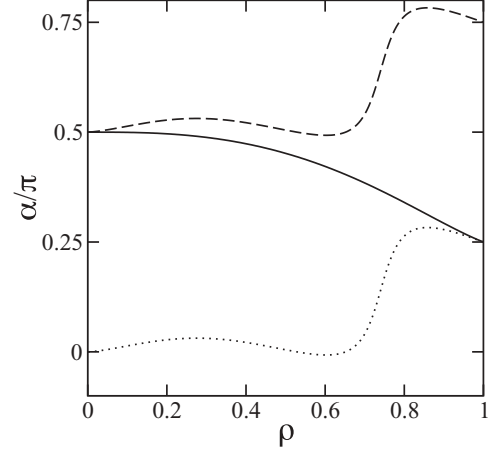

FIG. 5. The polar angle α (divided by π) of various 2D vectors as a function of the dimensionless size ratio ρ between the two layers. The solid line represents $\hat{\mathbf{s}}$, while the dotted and the dashed lines represent $\mathbf{d}_1$ and $\mathbf{d}_2$, respectively. We chose the value $Br_2^3/\kappa = 150$.

where $\hat{\mathbf{s}}$ is along the $(1,1)$ direction. In terms of the polar angle α between $\hat{\mathbf{s}}$ and the first axes on the $(r_1^2 u_1, r_2^2 u_2)$ plane, the $(1,1)$ direction corresponds to $\alpha = \pi/4$. Notice that this direction also corresponds to the undulation eigenmode direction. Since the sum of the two viscosity amplitudes is roughly a constant, as shown in Eq. (40), the slow squeezing mode takes a small viscosity amplitude η_2 for $\rho \approx 1$. In the other limit of $\rho \approx 0$, the shear mainly perturbs the outer layer. In this limit, we have $\hat{\mathbf{s}} = (0,1)$ or $\alpha = \pi/2$, and the slow mode is due to the outer layer relaxation. As a result, η_2 becomes the dominant contribution for $\rho \approx 0$. In Fig. 5, we plot the angle α as a function of ρ. The shear vector $\hat{\mathbf{s}}$ always coincides with the fast mode at $\rho = 1$ and the slow mode at $\rho = 0$. Therefore, the mode switching always takes place between $0 \leqslant \rho \leqslant 1$. It is also worth mentioning that Figs. 4 and 5, like Fig. 2, are plotted by assuming a constant B. These plots are used to analyze the behavior of the mode amplitudes. The more physical plots will be the ones using a suitable function for B.

Here we define a crossover size ratio ρ^* at which the two modes have the same viscosity amplitude, i.e., $\eta_1 = \eta_2$. In Fig. 6, we plot the calculated ρ^* as a function of Br_2^3/κ. When $Br_2^3/\kappa \ll 1$, the crossover happens at $\rho^* \approx 0.52$. This means that for the noninteracting case $B = 0$, the crossover happens when $d = r_2 - r_1$ is roughly the same as r_1. When $Br_2^3/\kappa \gg 1$, on the other hand, ρ^* approaches unity. As mentioned in Eq. (32), the parameter Br_2^3/κ will have a noticeable effect only when it is greater than 72. At the lower right corner of Fig. 6, where the layer interaction is strong and the layer separation is not too small, the slow mode has the dominant viscosity contribution. At the upper left corner where the layer interaction is relatively weak, the fast mode is more excited as compared to the slow mode.

VII. DISCUSSION

We have determined the crossover ration ρ^* in Fig. 6. The actual bilayer interaction strength B depends on the separation $d = r_2(1 - \rho)$. For the qualitative discussion at nonsmall ρ, we use the flat layer results in Sec. III B. In Fig. 7 we
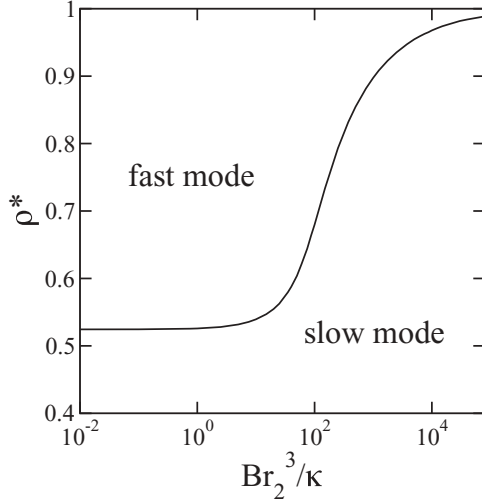
FIG. 6. The crossover size ratio ρ^* as a function of the dimensionless bilayer interaction Br_2^3/κ. For $\rho > \rho^*$, the fast mode is the dominant contribution to the viscosity, while the slower relaxation is dominant for $\rho < \rho^*$.

present both information in the $(\rho, Br_2^3/\kappa)$ plot to compare a series of systems with the same outer bilayer size r_2 but with different size ratios ρ. As one varies ρ, the dimensionless bilayer interaction strength Br_2^3/κ changes according to the DLVO theory Eq. (17) (two convex blue lines) or the Helfrich repulsion Eq. (18) (two concave red lines). If such lines happen to cross the line ρ^* (thick black line), one expects that the two viscosity amplitudes change their relative magnitudes. We have indicated such scenarios by the dashed lines.

As shown in the convex blue dashed line in Fig. 7, an electrostatically stabilized system may get large B by having
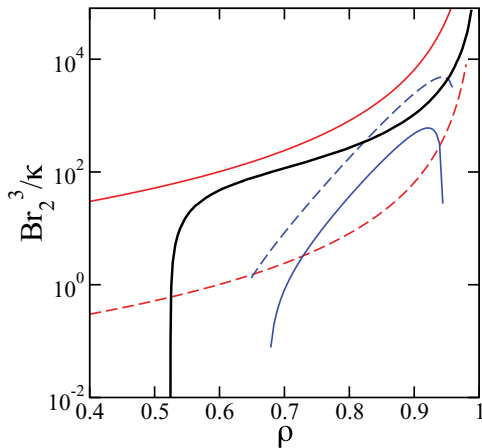

FIG. 7. (Color online) The dimensionless bilayer interaction Br_2^3/κ as a function of the size ratio ρ. The crossover ratio ρ^* in Fig. 6 is plotted by the thick solid black line. The two convex blue lines are from the DLVO theory Eq. (17) with $C_s = 0.01$ M, $\kappa_D = 3 \times 10^{-8}$ m, $A = 10^{-21}$ J, $\delta = 3 \times 10^{-9}$ m, and $k_BT = 4 \times 10^{-21}$ J. The surface potentials are 12 and 24 mV for the convex blue thin solid and dashed lines, respectively. The concave red lines are the Helfrich repulsion Eq. (18) with $c_0 = 36/\pi^2$, $r_2 = 10^{-7}$ m. The concave red thin solid and dashed lines are for $\kappa = 0.75k_BT = 3 \times 10^{-21}$ J and $\kappa = 7.5k_BT = 3 \times 10^{-20}$ J, respectively.

a high surface charge density. At small gap, the van der Waals attraction may also lower B, causing an interesting multiple crossing. This means that the viscosity amplitudes switch their magnitudes more than once. For a sterically stabilized system (concave red lines), we find that the dimensionless interaction parameter depends strongly on the bending rigidity as $Br_2^3/\kappa \sim \kappa^{-2}$ [see Eq. (18)]. For a soft surfactant bilayer of $\kappa = 0.75k_BT$, we find that the slow mode always dominates the viscosity. Whereas for a lipid bilayer whose bending rigidity $\kappa = 7.5k_BT$ is one order of magnitude larger, the concave red dashed line indicates that the squeezing mode is not much excited by shear when $\rho > 0.526$.

Caution should be kept when analyzing the MLV when ρ is close to unity. When the gap $d = r_2 - r_1$ is smaller than the distortion amplitude $|u_1| + |u_2|$, our result should be modified by the extra steric constraint, $r_1 + u_1 \leqslant r_2 + u_2$. Given a small but finite gap d, our linear calculation should be valid for small distortion amplitudes, $|u_1| + |u_2| < d$. This means that the linear response regime is restricted by the gap. As ρ becomes closer to unity (or $d \to 0$), the linear regime shrinks toward zero. Nonetheless, at a given ρ (but $\rho \neq 1$), our result should still be valid within the linear regime.

In this paper, we have only presented the calculation for two-layer vesicles. For MLV with more than two layers, the calculation can be performed in the same procedure but with a greater algebraic complexity [26]. For MLV with N layers, we expect that there are N relaxation modes. When the gap is small ($r_{N-1}/r_N \approx 1$), we expect that the majority of the N relaxations to bear some resemblance to the squeezing mode or the spherical version of the "slip mode" [11]. For larger gap, on the other hand, the relaxations of the N layers may decouple from each other. As for the viscoelasticity, we speculate that the viscosity amplitudes of the squeezing modes are small for weakly interacting MLV. Neutral or weakly charged lipid MLV should be an interesting system to investigate in this direction.

In polymer rheology calculation, one may consider a step strain for $t \geqslant 0$, where the time relaxation of the stress gives the relaxation modulus $G(t)$. This quantity can be further converted to the complex modulus $G^*(\omega)$ by the Fourier transform. Right after the step strain, one often assumes that the polymer deforms in an affine way [27]. Do we implicitly use the affine deformation approximation for the MLV rheology? A step strain for vesicle solution will induce a short but fast bilayer movement, where the **D** terms dominate the left-hand side of Eq. (19). Therefore, the initial layer displacements will be proportional to $\mathbf{D}^{-1} \cdot \hat{\mathbf{e}}_2 \propto (-D_{12}/D_{11}, 1)$, which is compatible with the incompressible constraints [see Eq. (B1)] at both layers. In the small gap limit, $\mathbf{D}^{-1} \cdot \hat{\mathbf{e}}_2$ behaves like $(\rho^2, 1)$. Compared with the affine deformation $u_n \propto r_n$, or in terms of our chosen variables $(r_1^2 u_1, r_2^2 u_2) \propto (\rho^3, 1)$, it is clear that our theory does not use the affine deformation approximation.

VIII. SUMMARY

In this work, we have calculated the slow relaxation rates and the viscoelasticity of a dilute two-layer-vesicle solution. In the model, the two vesicles are assumed to have the spherical equilibrium shape, which makes the analytic flow field tractable. We focus our discussion in the case where there

is no osmotic pressure so the tension for both layers vanishes. We also restrict our discussion to the case where the fluid in the three compartment has the same viscosity. To relax these two restrictions does not require a new calculation. Should a need arise, the present calculation procedure can be carried to those cases without any technical difficulty. Nonetheless, the commonly encountered situations often obey these two restrictions.

We have found the following results. (i) When the gap between two vesicles is small, the two relaxation modes consist of a combination between the squeezing and undulation characters. The former involves the opposite layer distortions, where the layer interaction drive the lubrication flow between the two layers as expressed in Eq. (31). The latter, calculated in Eq. (29), describes a relaxation driven by the layer bending elasticity, whereas the lubrication flow is not required. We find that for MLV with a small gap ($\rho \approx 1$), the slowest mode is the squeezing mode for which the Poiseuille flow mobility vanishes at the limit $\rho \to 1$. The undulation mode appears to be faster at a small gap.

(ii) At the other limit where the inner bilayer radius is small $\rho \approx 0$, it is easier to understand the relaxation in terms of the original variables u_1 and u_2. Here the slow mode becomes the relaxation of the outer bilayer, Eq. (32), and the faster mode is the relaxation of the inner bilayer, Eq. (30).

(iii) When one decreases ρ, the relaxation spectrum changes from (i) to (ii). The two dispersions change their characters with ρ to avoid the relaxation rate crossing. The slow mode can be approximated by Eq. (34) for the full range of ρ, where an adiabatic approximation for the fast u_1 variable is made. When the gap is mall, the slow mode is the squeezing mode. As the gap increases, the slow mode eventually becomes the outer layer relaxation mode.

(iv) At the low-frequency limit, the real part of the complex viscosity approaches that of the corresponding hard-sphere reference system. On the other hand, the real part of the complex viscosity shows that the high-frequency viscosity increment is between 12 and 16% of the hard-sphere viscosity increment. The difference between the two limits comes from the contributions of the two relaxation modes discussed above.

(v) For a fixed interaction strength Br_2^3/κ, we find that there is a crossover size ratio ρ^* which describes the crossover gap size. The slow mode is more difficult to excite when the gap is smaller than ρ^*. At a small gap, $\rho > \rho^*$, the slow (squeezing) mode has a small viscosity amplitude, while the fast (undulation) mode has a large viscosity amplitude. For large gap, $\rho < \rho^*$, on the other hand, the slow mode has the dominant viscosity amplitude. This shows that, for the MLV with small gaps, the slow mode is not the most important mode for viscoelasticity. In other words, the shear is not efficient to excite the slow mode when the gap is too small.

(vi) The crossover size ratio ρ^* depends on the interaction between the two bilayers. If Br_2^3/κ increases, ρ^* will increase from 0.52 toward unity. The interaction parameter B can be tuned, e.g., by adding block copolymers [28]. For strongly interacting MLV which has large Br_2^3/κ, the crossover gap is vanishingly small ($\rho^* \to 1$) so the slow mode is important for viscoelasticity. For noninteracting MLV, the crossover gap is $0.48r_2$, about half of the outer bilayer radius. In this weakly or noninteracting case there should be a higher possibility of

finding MLV whose viscoelasticity is dominated by the faster interbilayer relaxation. For neutral bilayers whose interaction arises from the Helfrich repulsion, the more rigid lipid system with a smaller gap might be a good candidate to observe the fast-mode-dominated viscoelasticity, as discussed in Fig. 7. For charged bilayers, a weakly charged system can also be used for such study. As suggested in a recent theoretical paper [26], the shear excited squeezing modes are important for MLV size selection. It will be interesting to study a lamellar system where the squeezing mode cannot be excited efficiently by shear.

APPENDIX A: SOLUTION OF STOKES EQUATION

For the incompressible solenoidal flow, the velocity can be expressed as

$$\mathbf{v} = \nabla \times (\nabla \psi \times \mathbf{r}) + \nabla \times (\zeta \mathbf{r}), \tag{A1}$$

where the scalar functions ψ and ζ are the defining function for the poloidal and toroidal flow fields, respectively. Note that our definition of the defining function differs by a factor r compared with the ones in the book by Chandrasekhar [29].

For an incompressible fluid, the divergence of the pressure gradient vanishes, i.e.,

$$\nabla^2 p = 0. \tag{A2}$$

Therefore, the pressure gradient is also a solenoidal field and can be described by the above decomposition. Since the toroidal part can be written as $(\nabla \zeta) \times \mathbf{r}$, the condition $\partial_\theta(\partial_\varphi p) = \partial_\varphi(\partial_\theta p)$ requires that $\partial_\theta(-\sin\theta \ \partial_\theta \zeta) = \partial_\varphi(\partial_\varphi \zeta / \sin\theta)$ or $\hat{L}^2 \zeta = 0$, where

$$\hat{L}^2 = -\frac{1}{\sin\theta}\frac{\partial}{\partial\theta}\left(\sin\theta\frac{\partial}{\partial\theta}\right) - \frac{1}{\sin^2\theta}\frac{\partial^2}{\partial\varphi^2}. \tag{A3}$$

Hence, the pressure gradient is only poloidal and written as

$$\nabla p = \nabla \times (\nabla \Psi \times \mathbf{r})$$
$$= \hat{r}\frac{\hat{L}^2\Psi}{r} + \hat{\theta}\frac{1}{r}\frac{\partial}{\partial\theta}\frac{\partial(r\Psi)}{\partial r} + \hat{\varphi}\frac{1}{r\sin\theta}\frac{\partial}{\partial\varphi}\frac{\partial(r\Psi)}{\partial r}, \tag{A4}$$

where Ψ is the defining function of ∇p. Comparing the $\hat{\theta}$ and $\hat{\varphi}$ directions, we can set

$$p = \frac{\partial(r\Psi)}{\partial r} \tag{A5}$$

for these two directions. The Laplace equation for the pressure Eq. (A2) then implies that

$$\frac{1}{r^2}\frac{\partial}{\partial r}\left(r^2\frac{\partial^2(r\Psi)}{\partial r^2}\right) - \frac{\hat{L}^2}{r^2}\frac{\partial(r\Psi)}{\partial r} = 0. \tag{A6}$$

Therefore, the radial component of the gradient pressure can be either expressed as $\hat{L}^2\Psi/r$ or $\partial_r^2(r\Psi)$. The latter expression is consistent with the identification Eq. (A5).

For the velocity field, we will drop the toroidal part by setting $\zeta = 0$. This is justified because the tangential force field is a surface gradient and drives only the poloidal flow. To obtain the defining function ψ, we take the curl of Eq. (5) to get $\nabla \times \nabla^2 \mathbf{v} = 0$. Since $\nabla^2 \mathbf{v} = -\nabla \times \nabla \times \mathbf{v}$ holds for incompressible flow, we have

$$\nabla \times \nabla \times \nabla \times \nabla \times [\nabla \times (\psi \mathbf{r})] = 0, \qquad (A7)$$

where, in the square bracket, an equivalent form of $\nabla\psi \times \mathbf{r}$ is used. As detailed in Ref. [29], each curl will switch poloidal and toroidal parts. The double curl will preserve the type and modify the defining function by $-\nabla^2$. The curl of Eq. (5) becomes $\nabla \times (\mathbf{r}\nabla^4\psi) = 0$ or

$$\nabla^4\psi = 0. \qquad (A8)$$

To find the coupling between the pressure p and the velocity poloidal function ψ in Eq. (5), we rewrite $-\nabla^2\mathbf{v} = \nabla \times \nabla \times \mathbf{v} = \nabla \times [\nabla(-\nabla^2\psi) \times \mathbf{r}]$. Equation (5) then is satisfied when

$$-\Psi + \eta\nabla^2\psi = 0.$$

Here we prefer to use p instead of Ψ. Operating the above equation by $\hat{L}^2/r$ and substituting the combination $\hat{L}^2\Psi/r$ by $\partial_r p$, we obtain

$$r\frac{\partial p}{\partial r} = \eta\hat{L}^2\nabla^2\psi. \qquad (A9)$$

Using the standard method of separation of variables, the general solution of Eqs. (A2), (A8), and (A9) are

$$p = p_0 + \sum_{lm}\left(p_{lm}^{\mathrm{I}}r^l + p_{lm}^{\mathrm{II}}r^{-l-1}\right)Y_{lm}, \qquad (A10)$$

$$\psi = \sum_{lm}\left(\psi_{lm}^{\mathrm{I}}r^l + \psi_{lm}^{\mathrm{II}}r^{-l-1}\right)Y_{lm}$$
$$+ \sum_{lm}\left(\frac{p_{lm}^{\mathrm{I}}r^{l+2}}{\eta(2l+2)(2l+3)} + \frac{p_{lm}^{\mathrm{II}}r^{-l+1}}{2\eta l(2l-1)}\right)Y_{lm}, \qquad (A11)$$

where $Y_{lm}(\theta,\varphi)$ are the spherical harmonics.

APPENDIX B: THE SURFACE INCOMPRESSIBLE LIMIT

The surface incompressibility condition also constrains the velocity field as

$$\frac{2v_r(r_n)}{r} + \nabla_\perp \cdot \mathbf{v}_\perp(r_n) = 0 \qquad (B1)$$

at both $r = r_1$ and r_2. Because the fluid is incompressible, i.e., $\nabla \cdot \mathbf{v} = 0$, Eq. (B1) can also be expressed as the equivalent form,

$$\frac{\partial v_r(r_n)}{\partial r} = 0, \qquad (B2)$$

at the bilayers. We prefer this condition because it simplifies the calculation.

We now consider the relaxation rates of a small perturbation described by the spherical harmonics $Y_{lm}(\theta,\varphi)$. To simplify the notation, we drop the subscript "lm" of the coefficients ψ_{lm}^{I}, ψ_{lm}^{II}, p_{lm}^{I}, and p_{lm}^{II}. For the region within the bilayer 1

$(0 \leqslant r \leqslant r_1)$, we set $\psi_{lm}^{\mathrm{II}} = 0$ and $p_{lm}^{\mathrm{II}} = 0$ to drop the functions which are singular at $r = 0$. We denote ψ_{lm}^{I} and p_{lm}^{I} as $\psi_{\mathrm{A}}^{\mathrm{I}}$ and $p_{\mathrm{A}}^{\mathrm{I}}$, respectively. The 2D incompressibility condition Eq. (B2) relates the two remaining coefficients as

$$\psi_{\mathrm{A}}^{\mathrm{I}} = \frac{r_1^2}{2\eta(2l+3)(l-1)}p_{\mathrm{A}}^{\mathrm{I}}. \qquad (B3)$$

In terms of the radial velocity amplitude v_1, we can further express the pressure coefficient as

$$p_{\mathrm{A}}^{\mathrm{I}} = -\frac{\eta(2l+3)(l-1)r_1^{-l-1}}{l}v_1. \qquad (B4)$$

For the region exterior to the bilayer 2 ($r_2 \leqslant r < \infty$), the coefficients ψ_{lm}^{I} are zero, except ψ_{20}^{I}, which needs to be chosen to give the far flow Eq. (8). Comparing the radial component v_r from Eq. (8) and $\hat{L}^2\psi/r$, we set $\psi_{20}^{\mathrm{I}} = \Gamma/3$. We also set $p_{lm}^{\mathrm{I}} = 0$ so p does not diverge at $r \to \infty$, and denote ψ_{lm}^{II} and p_{lm}^{II} as $\psi_{\mathrm{C}}^{\mathrm{II}}$ and $p_{\mathrm{C}}^{\mathrm{II}}$, respectively. Then the 2D incompressibility condition Eq. (B2) relates the two remaining coefficients as

$$\psi_{\mathrm{C}}^{\mathrm{II}} = -\frac{r_2^2}{2\eta(2l-1)(l+2)}p_{\mathrm{C}}^{\mathrm{II}} + \frac{1}{12}r_2^5\Gamma\delta_{l2}\delta_{m0}. \qquad (B5)$$

Using the radial velocity amplitude v_2, we can express the pressure coefficient as

$$p_{\mathrm{C}}^{\mathrm{II}} = \frac{\eta(2l-1)(l+2)r_2^l}{l+1}v_2 - 10\eta r_2^3\Gamma\delta_{l2}\delta_{m0}. \qquad (B6)$$

For the region between the two bilayers ($r_1 \leqslant r < r_2$), the expressions are more complex. The incompressibility Eq. (B2), evaluated at r_1 and r_2, provides two conditions between the four coefficients,

$$\psi_{\mathrm{B}}^{\mathrm{I}} = F_{11}p_{\mathrm{B}}^{\mathrm{I}} + F_{12}p_{\mathrm{B}}^{\mathrm{II}},$$
$$\psi_{\mathrm{B}}^{\mathrm{II}} = F_{21}p_{\mathrm{B}}^{\mathrm{I}} + F_{22}p_{\mathrm{B}}^{\mathrm{II}}, \qquad (B7)$$

where

$$F_{11} = -\frac{r_2^{2l+3} - r_1^{2l+3}}{2\eta(2l+3)(l-1)\left(r_2^{2l+1} - r_1^{2l+1}\right)},$$
$$F_{12} = \frac{r_2^2 - r_1^2}{2\eta(2l-1)(l-1)\left(r_2^{2l+1} - r_1^{2l+1}\right)},$$
$$F_{21} = -\frac{r_1^{2l+1}r_2^{2l+1}\left(r_2^2 - r_1^2\right)}{2\eta(2l+3)(l+2)\left(r_2^{2l+1} - r_1^{2l+1}\right)}, \qquad (B8)$$
$$F_{22} = -\frac{r_1^2 r_2^{2l+1} - r_2^2 r_1^{2l+1}}{2\eta(2l-1)(l+2)\left(r_2^{2l+1} - r_1^{2l+1}\right)}.$$

We prefer to use the variables v_1 and v_2 instead of $p_{\mathrm{B}}^{\mathrm{I}}$ and $p_{\mathrm{B}}^{\mathrm{II}}$. The pressure coefficients then can be expressed as

$$p_{\mathrm{B}}^{\mathrm{I}} = G_{11}v_1 + G_{12}v_2,$$
$$p_{\mathrm{B}}^{\mathrm{II}} = G_{21}v_1 + G_{22}v_2, \qquad (B9)$$

where

$$G_{11} = \frac{\eta}{lG_0}\left\{(-8l^2 - 4l + 12)r_1^{3l+2}r_2 \right.$$
$$\left. - (4l+6)r_1^{l+1}r_2^{2l}\left[l(2l+1)r_1^2 - (l+2)(2l-1)r_2^2\right]\right\},$$

$$G_{12} = \frac{\eta}{lG_0}\Big\{(-8l^2 - 4l + 12)r_1 r_2^{3l+2}$$
$$- (6l+4)r_1^{2l} r_2^{l+1}\big[l(2l+1)r_2^2 - (l+2)(2l-1)r_1^2\big]\Big\},$$

$$G_{21} = \frac{(4l-2)\eta}{(l+1)G_0}\Big\{-(2l^2+3l+1)r_1^{3l+4}r_2^{2l}$$
$$+ (2l^2+l-3)r_1^{3l+2}r_2^{2l+2} + (2l+4)r_1^{l+1}r_2^{4l+3}\Big\},$$

$$G_{22} = \frac{(4l-2)\eta}{(l+1)G_0}\Big\{-(2l^2+3l+1)r_2^{3l+4}r_1^{2l}$$
$$+ (2l^2+l-3)r_2^{3l+2}r_1^{2l+2} + (2l+4)r_2^{l+1}r_1^{4l+3}\Big\},$$
$$\text{(B10)}$$

with

$$G_0 = r_2^{4l+4}[4\rho + 4\rho^{4l+3} - (2l+1)^2\rho^{2l+4}$$
$$- (6 - 8l - 8l^2)\rho^{2l+2} - (2l+1)^2\rho^{2l}]. \quad \text{(B11)}$$

When the two bilayer are well separated ($r_1 \ll r_2$), both G_{11} and G_{22} become small. In this limit, G_{12} becomes the coefficient of Eq. (B4) with r_1 replaced by r_2, whereas G_{21} becomes the coefficient of Eq. (B6) (without the Γ term) with r_2 replaced by r_1.

APPENDIX C: THE STRESS AND THE TENSION PERTURBATION

The radial component of the normal stress appears in Eq. (6). From its component form $\sigma_{rr} = -p + 2\eta\partial_r v_r$ and the 2D incompressibility condition Eq. (B2), it is just the negative pressure. Therefore, the stress differences at the two bilayers are

$$\sigma_{rr}(r_1^+) - \sigma_{rr}(r_1^-) = \sum_{lm}\big[(p_A^I - p_B^I)r_1^l - p_B^{II}r_1^{-l-1}\big]Y_{lm},$$

$$\sigma_{rr}(r_2^+) - \sigma_{rr}(r_2^-) = \sum_{lm}\big[p_B^I r_2^l + (p_B^{II} - p_C^{II})r_2^{-l-1}\big]Y_{lm}.$$
$$\text{(C1)}$$

The large bilayer stretching modulus E suppresses the surface density perturbation. For the slow relaxation, we will take the limit $E \to \infty$ to eliminate the parameter E. Within this limit, both ϕ_1 and ϕ_2 approach unity, so the tension perturbations $\delta\gamma_1$ and $\delta\gamma_2$ become the Lagrange multipliers. The values of the Lagrange multipliers then are determined by Eqs. (7) and (11) instead of their original definitions, as discussed below.

In Eq. (7), we are interested in the difference between the tangential stress across the bilayer. We express the tangential stress as a function of ψ,

$$\sigma_\perp = \hat{\theta}\sigma_{r\theta} + \hat{\varphi}\sigma_{r\varphi} = \eta\nabla_\perp\left[r\frac{\partial^2\psi}{\partial r^2} + (\hat{L}^2 - 2)\frac{\psi}{r}\right]. \quad \text{(C2)}$$

We now replace $\partial_r^2\psi$ using Eq. (A9), and limit our discussion to the $l \neq 0$ mode. The velocity field $\nabla \times (\nabla\psi \times \mathbf{r})$ has components similar to those of Eq. (A4). We can use the r component $v_r = \hat{L}^2\psi/r$ to eliminate ψ as $(r/\hat{L}^2)v_r$ so

$$\sigma_\perp = \nabla_\perp\left[\frac{r^2}{\hat{L}^2}\frac{\partial p}{\partial r} + \eta\left(2 - \frac{4}{\hat{L}^2}\right)v_r - 2\eta\frac{r}{\hat{L}^2}\frac{\partial v_r}{\partial r}\right], \quad \text{(C3)}$$

where $\hat{L}^2 \to l(l+1)$ for spherical harmonics with nonzero l. Because v_r is continuous across the bilayer and $\partial_r v_r$ vanishes on the bilayer, only the first term can differ across the bilayer. This is the only important term for the tension perturbation in Eqs. (7) and (11),

$$\delta\gamma_n = -\frac{r_n^2}{\hat{L}^2}\left(\frac{\partial p}{\partial r}\right)_{r_n^+} + \frac{r_n^2}{\hat{L}^2}\left(\frac{\partial p}{\partial r}\right)_{r_n^-}. \quad \text{(C4)}$$

We then obtain

$$\delta\gamma_1 = \sum_{lm}\left(\frac{p_A^I - p_B^I}{l+1}r_1^{2l+1} + \frac{p_B^{II}}{l}r_1^{-l}\right)Y_{lm},$$

$$\delta\gamma_2 = \sum_{lm}\left(\frac{p_B^I}{l+1}r_2^{2l-1} + \frac{p_C^{II} - p_B^{II}}{l}r_2^{-l}\right)Y_{lm}.$$
$$\text{(C5)}$$

[1] J. S. Huang, S. T. Milner, B. Farago, and D. Richter, Phys. Rev. Lett. **59**, 2600 (1987).

[2] B. Farago, D. Richter, J. S. Huang, S. A. Safran, and S. T. Milner, Phys. Rev. Lett. **65**, 3348 (1990).

[3] M. B. Schneider, J. T. Jenkins, and W. W. Webb, J. Phys. (France) **45**, 1457 (1984).

[4] S. T. Milner and S. A. Safran, Phys. Rev. A **36**, 4371 (1987).

[5] A. Onuki and K. Kawasaki, Europhys. Lett. **18**, 729 (1992).

[6] K. Seki and S. Komura, Physica A **219**, 253 (1995).

[7] N. Robinson, J. Pharm. Pharmacol. **12**, 129 (1960).

[8] N. Robinson, J. Pharm. Pharmacol. **12**, 193 (1960).

[9] T. D. Le, U. Olsson, K. Mortensen, J. Zipfel, and W. Richtering, Langmuir **17**, 999 (2001).

[10] O. Diat and D. Roux, J. Phys. (France) II **3**, 9 (1993).

[11] F. Brochard and P.-G. de Gennes, Pramana Suppl. **1**, 1 (1975).

[12] F. Nallet, D. Roux, and J. Prost, J. Phys. (France) **50**, 3147 (1989).

[13] S. Ramaswamy, J. Prost, W. Cai, and T. C. Lubensky, Europhys. Lett. **23**, 271 (1993).

[14] G. Sigaud, C. W. Garland, H. T. Nguyen, D. Roux, and S. T. Milner, J. Phys. (France) II **3**, 1343 (1993).

[15] H. M. Fijnaut and J. G. H. Joosten, J. Chem. Phys. **69**, 1022 (1978).

[16] C. Y. Young and N. A. Clark, J. Chem. Phys. **74**, 4171 (1981).

[17] E. I. Kats, V. V. Lebedev, and S. V. Malinin, JETP **86**, 1149 (1998).

[18] An equilibrium lamellar phase does not have tension. For a lamellar phase that could swell, a metastable MLV will take up some solvent so tension is developed. For a lamellar phase at the dilute phase boundary, the layers can coexist with the excess solvent without further swelling. Therefore, the metastable MLV there is likely to have a negligible tension.

[19] G. K. Batchelor, J. Fluid Mech. **41**, 545 (1970).

[20] J. N. Israelachvili, *Intermolecular and Surface Forces*, 2nd ed. (Academic Press, New York, 1992).

[21] S. A. Safran, *Statistical Thermodynamics of Surfaces, Interfaces, and Membranes* (Addison-Wesley, Reading, MA, 1994).

[22] W. A. Russel, D. A. Saville, and W. R. Schowalter, *Colloidal Dispersions* (Cambridge University Press, Cambridge, UK, 1989).

[23] V. A. Parseigian, *Van der Waals Forces: A Handbook for Biologists, Chemists, Engineers, and Physicists* (Cambridge University Press, Cambridge, UK, 2005).

[24] W. Helfrich, Z. Naturforsch. **33a**, 305 (1978).

[25] R. Lipowsky and S. Leibler, Phys. Rev. Lett. **56**, 2541 (1986).

[26] C.-Y. D. Lu, Phys. Rev. Lett. **109**, 128304 (2012).

[27] M. Doi and S. F. Edwards, *The Theory of Polymer Dynamics* (Clarendon Press, Oxford, 1986).

[28] S. Fujii, S. Koschoreck, P. Lindner, and W. Richtering, Langmuir **25**, 5476 (2009).

[29] S. Chandrasekhar, *Hydrodynamic and Hydromagnetic Stability* (Clarendon, Oxford, 1961).